Aalborg Universitet

AALBORG UNIVERSITY

DENMARK

Constrained Modulated Model-Predictive Control of an LC-Filtered Voltage-Source Converter

Zheng, C.; Dragicevic, T.; Majmunovic, B.; Blaabjerg, F.

Constrained Modulated-Model Predictive Control of an *LC*-Filtered Voltage Source Converter

Changming Zheng, *Student Member, IEEE*, Tomislav Dragičević, *Senior Member, IEEE*,
Branko Majmunović, *Student Member, IEEE*, and Frede Blaabjerg, *Fellow, IEEE*

Abstract—This paper proposes a constrained modulated-model predictive control (M^2PC) scheme for an *LC*-filtered voltage source converter (VSC). To tackle the coupling effects of the state variables in a second-order *LC* filter, a dual-objective cost function (CF) is used to explicitly track both capacitor voltage and inductor current references, which can achieve an improved voltage quality. To handle the state and control input constraints of VSCs, a constrained M^2PC scheme is proposed with an 'online post-correction' constraint-handling technique. First, the unconstrained optimal voltage vector (OVV) is derived. It is generated by seeking the minimum analytical solution of the CF offline, simplifying the online implementation. Then, an 'online post-correction' strategy is employed by reconsidering the constraints to correct the precalculated OVV online, which guarantees the future states within the allowed range. Finally, the corrected OVV is synthesized by the space vector modulation (SVM), resulting in a fixed switching frequency and low harmonics. Compared with the typical constrained MPC, the presented scheme has the advantages of improved steady-state performance, flexible constraint-handling ability and lower computational cost. Additionally, design procedures for weighting factor (WF) selection in the CF are given. Comparative experiments are investigated to verify the presented control strategy.

Index Terms—Voltage source converter (VSC), *LC* filter, model predictive control (MPC), constraints, modulation.

I. INTRODUCTION

THREE-PHASE voltage source converters (VSCs) are the key interfaces for energy transmission between a dc stage and a standalone ac load or the grid. An *LC*-filtered VSC is a commonly-used topology to obtain a low total-harmonic-distortion (THD) output voltage, which has been extensively applied in distributed generation (DG) systems, stand-alone operation of AC microgrids (MGs), energy storage systems (ESSs) and also the uninterruptible power supply (UPS) systems [1]–[3].

Various control algorithms have been presented for improving the operation performance of the *LC*-filtered VSCs, including multiloop proportional integral (PI) or proportional resonant (PR) control [4], [5], dead-beat control [6], repetitive control and sliding mode control (SMC) [7]. Recently, owing

to the explosive evolution of the fast microprocessors, model predictive control (MPC) has gained increasing attention in the converter and motor control due to the following merits: intuitive implementation, fast dynamic response, and high flexibility to include various constraints and nonlinearities [8]. The fundamental of MPC is based on the predictive model, predicting the system behavior by selecting the optimal control input among all feasible ones over finite future horizons [9]. The optimal control input is obtained by minimizing a cost function (CF) that involves multiple control objectives and then applied to the converters. According to the ways of generating control inputs, MPC is broadly grouped into finite control-set MPC (FCS-MPC) and continuous control-set MPC (CCS-MPC) [10]–[12].

FCS-MPC makes the most out of the discretized essence of VSCs, it considers only the finite switching combinations for the system behavior prediction. The predefined CF is evaluated using each predictions and the minimal-cost switching combination is chosen and employed. The attractive features of FCS-MPC are that no modulation stage is needed, and the multi-objective control and constraints can easily be included in CF without increasing too much the computational complexity. Hence, this control strategy is feasible to execute online and has been extensively utilized in power converters [13]–[15]. However, lack of the modulator causes a non-constant switching frequency, which degrades the steady-state performance, resulting in increased switching losses and spread harmonic spectra [16]. To overcome these drawbacks, several solutions have been proposed either by taking into account the harmonic spectrum shaping in CF [17], or introducing suitable modulation concepts to mimic the behavior of constant switching frequency [18], [19]. Another issue of this approach is the unneglectable steady-state error, particularly under low switching frequency or small references. It can be mitigated by using different sampling frequencies or considering the intersampling errors [20].

The other family is CCS-MPC, which generates the control input in a continuous form instead of the finite switching states [11], [21]. Typically, a modulator is exploited to synthesize the optimal voltage vector (OVV). The major merits of this strategy are the flexible inclusion of multiple control objectives and the constant switching frequency [21]. These advantages enable the CCS-MPC to exhibit a better steady-state performance with a lower THD and to facilitate the filter design in comparison to FCS-MPC. One favorable control strategy in this family, generalized predictive control (GPC), is a transfer-function based approach that is possible to implement

online [11]. It is suitable for long prediction horizons but difficult to tackle its constraints [9], [22]. With regards to multiple constraints, typical CCS-MPC usually needs to solve a quadratic program (QP) problem online [9]. This leads to a considerable computational burden compared with the unconstrained situation, making it hard to implement using commercial control platforms. One solution is the explicit MPC (EMPC), which can solve the QP problem off-line, yielding a lookup table [23]. Nevertheless, its computational complexity is exponentially increased with the number of state variables and constraints, and a large memory space for storing the lookup tables is needed, making it inapplicable for multi-constraints situations [24]. In contrast, [25] proposes a computationally efficient implicit MPC by indirectly merging different constraints according to their relationships. However, it is based on the three-phase natural coordinate system, the optimization calculation needs to be repeated for each of the three phases separately, increasing the computational efforts to some degree. Meanwhile, it only gives the simulation results while the inherent digital control delay is not considered, which leads to the failure of this approach practically. Moreover, in terms of the α-β control frame based VSCs, the constraints are usually quadratic instead of the linear inequalities, which may increase the computational complexity of the aforementioned approaches.

Other critical issues about MPC are the CF design and the weighting factors (WFs) selection. Both FCS-MPC and CCS-MPC can easily include multiple control objectives in the CF, and these objective terms are normally balanced by the WFs [26]. For *LC*-filtered VSCs, the commonly-used primary term is the voltage tracking term, and the equally important term is scarcely included both in typical FCS-MPC and CCS-MPC [2], [25]. However, the single voltage tracking objective cannot achieve satisfactory control performance due to the coupling effects between the inductor current and the capacitor voltage [27]. By adding a voltage-derivative tracking term in CF, a modified FCS-MPC strategy is proposed, offering a better voltage quality [27]. However, this modified strategy still inherits the disadvantages of non-constant switching frequency and spread harmonic spectrum since it is based on FCS-MPC. In addition, the WFs selection in FCS-MPC is an established open issue and the commonly-used method is trial-and-error [26]. Recently, several approaches have been proposed to select the WFs automatically [28], [29], avoiding the time-consuming manual selection. In contrast, since the CCS-MPC is inherently a linear control strategy, it is possible to select the WFs using linear analysis methods. Nevertheless, little research has systematically reported the analytical procedures of the WF selection for CCS-based MPC schemes.

This paper presents a constrained modulated model predictive control (M²PC) of an *LC*-filtered VSC. The OVV is obtained by calculating the minimal analytical solution of CF and synthesized by space vector modulation (SVM), resulting in a fixed switching frequency. The core contributions are generalized as below:

1) A dual-objective CF including the inductor current tracking objective as an 'equally important term' is introduced, which achieves 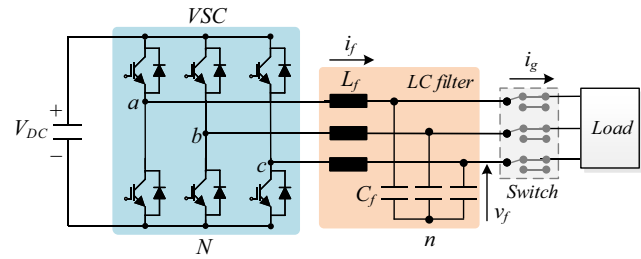an improved voltage quality (lower steady-state tracking error and THD) in comparison to modified FCS-MPC and typical CCS-MPC [25], [27].

2) A constrained M²PC scheme with an 'online post-correction' constraint-handling strategy is proposed. Compared with the state of art of the CCS-based MPC scheme, the proposed scheme offers a lower computational cost.

3) Specific procedures for the WF selection of M²PC and sensitivity analysis to model mismatch are intuitively given.

The remainder of the work is arranged as follows: The discrete predictive model of *LC*-filtered VSC is derived in Section II. Section III explains the principle of the presented scheme, and Section IV provides the WF selection procedures. Section V elaborates the experimental results and analysis, and the conclusion is given in Section VI .

II. DISCRETE PREDICTIVE MODEL OF THE SYSTEM

A typical topology of the widely-used three phase *LC*-filtered VSC is illustrated in Fig. 1. The *LC* filter with balanced inductor L_f and capacitor C_f connected in each phase, is the key component to reduce the voltage harmonic content of VSCs. To implement the model-based MPC, the discrete predictive model is required. Fig. 2 depicts the *LC* filter model in *s*-domain, and the continuous-time dynamics of *LC* filter is described as

$$\begin{cases} L_f \dfrac{d\bar{i}_f}{dt} = \bar{v}_i - \bar{v}_f \\ C_f \dfrac{d\bar{v}_f}{dt} = \bar{i}_f - \bar{i}_g \end{cases} \tag{1}$$

with the complex variables in the α-β coordinate system [27]

$$\begin{cases} \bar{v}_f = v_{f\alpha} + jv_{f\beta}, \bar{v}_i = v_{i\alpha} + jv_{i\beta} \\ \bar{i}_f = i_{f\alpha} + ji_{f\beta}, \ \bar{i}_g = i_{g\alpha} + ji_{g\beta} \end{cases} \tag{2}$$

where $\bar{v}_f$, $\bar{i}_f$, $\bar{v}_i$ and $\bar{i}_g$ represent the capacitor voltage, inductor current, converter voltage vector and the load current in the complex form.

Fig. 1. Typical topology of an *LC*-filtered VSC.
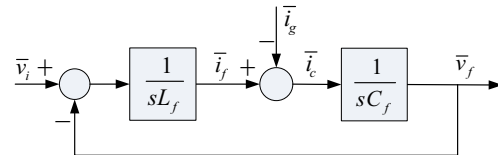
Fig. 2. Block diagram of *s*-domain *LC* filter model in the complex α-β coordinate system.

To facilitate the analysis, (1) is expressed as a continuous-time state space model form

$$\frac{d}{dt}\begin{bmatrix}\bar{i}_f \\ \bar{v}_f\end{bmatrix} = \mathbf{\Phi_c}\begin{bmatrix}\bar{i}_f \\ \bar{v}_f\end{bmatrix} + \mathbf{\Gamma_c}\bar{v}_i + \mathbf{\Gamma_{gc}}\bar{i}_g \tag{3}$$

where

$$\mathbf{\Phi_c} = \begin{bmatrix} 0 & -\frac{1}{L_f} \\ \frac{1}{C_f} & 0 \end{bmatrix}, \mathbf{\Gamma_c} = \begin{bmatrix} \frac{1}{L_f} \\ 0 \end{bmatrix}, \mathbf{\Gamma_{gc}} = \begin{bmatrix} 0 \\ -\frac{1}{C_f} \end{bmatrix}.$$

Correspondingly, utilizing the zero order holder, the discretized predictive model is formulated as [2]

$$\underbrace{\begin{bmatrix}\bar{i}_f(k+1) \\ \bar{v}_f(k+1)\end{bmatrix}}_{\bar{\mathbf{x}}(k+1)} = \underbrace{\begin{bmatrix}\Phi_{11} & \Phi_{12} \\ \Phi_{21} & \Phi_{22}\end{bmatrix}}_{\mathbf{\Phi_d}}\underbrace{\begin{bmatrix}\bar{i}_f(k) \\ \bar{v}_f(k)\end{bmatrix}}_{\bar{\mathbf{x}}(k)} + \underbrace{\begin{bmatrix}\Gamma_{11} \\ \Gamma_{21}\end{bmatrix}}_{\mathbf{\Gamma_d}}\bar{v}_i(k) + \underbrace{\begin{bmatrix}\Gamma_{12} \\ \Gamma_{22}\end{bmatrix}}_{\mathbf{\Gamma_{gd}}}\bar{i}_g(k)$$

$$\tag{4}$$

with

$$\mathbf{\Phi_d} = e^{\mathbf{\Phi_c}T_s} \tag{5}$$

$$\mathbf{\Gamma_d} = \int_0^{T_s} e^{\mathbf{\Phi_c}\tau}\mathbf{\Gamma_c}d\tau \tag{6}$$

$$\mathbf{\Gamma_{gd}} = \int_0^{T_s} e^{\mathbf{\Phi_c}\tau}\mathbf{\Gamma_{gc}}d\tau \tag{7}$$

where $\bar{\mathbf{x}}$ is state variable matrix. $\mathbf{\Phi_d}$, $\mathbf{\Gamma_d}$ and $\mathbf{\Gamma_{gd}}$ are constant predictive matrices. T_s is the sampling period.

III. PROPOSED CONSTRAINED M²PC

For an *LC*-filtered VSC, the capacitor voltage is usually the primary control object in typical CF [2], [25]. However, its derivative is indirectly regulated by the inductor current instead of the converter's OVV due to *LC* filter's coupling effects [27]. Hence, control of the inductor current is also important for voltage quality enhancement, and it is included in the CF as an 'equally important term' together with the capacitor voltage tracking term, as described below.

A. Dual-Objective CF Design

Note that the capacitor voltage reference is sinusoidal, and it can be expressed as

$$\bar{v}_f^*(t) = \underbrace{V_{\text{ref}}\cos(\omega_{\text{ref}}t)}_{v_{f\alpha}^*(t)} + j\underbrace{V_{\text{ref}}\sin(\omega_{\text{ref}}t)}_{v_{f\beta}^*(t)} \tag{8}$$

where ω_{ref} and V_{ref} are the reference angular frequency and the reference capacitor voltage amplitude.

Considering the internal relationship between the inductor current and the capacitor voltage, the inductor current reference is given by [27]

$$\bar{i}_f^*(t) = C_f\frac{d\bar{v}_f^*(t)}{dt} + \bar{i}_g(t)$$
$$= \underbrace{-C_f\omega_{\text{ref}}v_{f\beta}^*(t) + i_{g\alpha}(t)}_{i_{f\alpha}^*(t)} + j\underbrace{(C_f\omega_{\text{ref}}v_{f\alpha}^*(t) + i_{g\beta}(t))}_{i_{f\beta}^*(t)}. \tag{9}$$

Corresponding discretized form of references (8) and (9) can be developed as

$$\begin{cases} \bar{v}_f^*(k) = V_{\text{ref}}\cos(\omega_{\text{ref}}kT_s) + jV_{\text{ref}}\sin(\omega_{\text{ref}}kT_s) \\ \bar{i}_f^*(k) = jC_f\omega_{\text{ref}}\bar{v}_f^*(k) + \bar{i}_g(k). \end{cases} \tag{10}$$

Hence, the dual-objective CF for explicitly tracking both capacitor voltage and inductor current is designed as

$$g_{dual} = g_{vf} + \lambda g_{if} \tag{11}$$

with the quadratic objective terms

$$\begin{cases} g_{vf} = (v_{f\alpha}^*(k+1) - v_{f\alpha}(k+1))^2 + (v_{f\beta}^*(k+1) - v_{f\beta}(k+1))^2 \\ g_{if} = (i_{f\alpha}^*(k+1) - i_{f\alpha}(k+1))^2 + (i_{f\beta}^*(k+1) - i_{f\beta}(k+1))^2 \end{cases} \tag{12}$$

where g_{vf} and g_{if} are the control objective terms. $\lambda > 0$ is the weighting factor. $v_{f\alpha}^*(k+1)$, $v_{f\beta}^*(k+1)$, $i_{f\alpha}^*(k+1)$ and $i_{f\beta}^*(k+1)$ are the reference values. $v_{f\alpha}(k+1)$, $v_{f\beta}(k+1)$, $i_{f\alpha}(k+1)$ and $i_{f\beta}(k+1)$ are the state predictions calculated by the predictive model (4).

B. Unconstrained M²PC and OVV Calculation

First, all of the system constraints are neglected. The primary target of the unconstrained M²PC is to find the OVV that can minimize the CF in (11), namely

$$\min_{v_{i\alpha}(k),v_{i\beta}(k)} g_{dual}(v_{i\alpha}(k), v_{i\beta}(k)). \tag{13}$$

Different from the discrete nature of FCS-MPC, the proposed M²PC is inherently a CCS-MPC based strategy. A simple method is used to solve (13), i.e., calculating its minimum analytical solution to generate the unconstrained OVV by

$$\begin{cases} \dfrac{\partial g_{dual}(v_{i\alpha}(k), v_{i\beta}(k))}{\partial v_{i\alpha}(k)} = 0 \\ \dfrac{\partial g_{dual}(v_{i\alpha}(k), v_{i\beta}(k))}{\partial v_{i\beta}(k)} = 0. \end{cases} \tag{14}$$

Substitute (11) and (12) into (14), after a necessary simplification, the two scalar components of the unconstrained OVV, $v_{i\alpha}^{\text{ref}}(k)$ and $v_{i\beta}^{\text{ref}}(k)$ are derived and can be written in a complex form as

$$\bar{v}_i^{\text{ref}}(k) = \mu_1\bar{i}_f(k) + \mu_2\bar{v}_f(k) + \mu_3\bar{i}_f^*(k+1) \\ + \mu_4\bar{v}_f^*(k+1) + \mu_5\bar{i}_g(k) \tag{15}$$

where the coefficients are

$$\begin{cases} \mu_1 = -\dfrac{\lambda\Gamma_{11}\Phi_{11} + \Gamma_{21}\Phi_{21}}{\lambda\Gamma_{11}^2 + \Gamma_{21}^2} \\ \mu_2 = -\dfrac{\lambda\Gamma_{11}\Phi_{12} + \Gamma_{21}\Phi_{22}}{\lambda\Gamma_{11}^2 + \Gamma_{21}^2} \\ \mu_3 = \dfrac{\lambda\Gamma_{11}}{\lambda\Gamma_{11}^2 + \Gamma_{21}^2} \\ \mu_4 = \dfrac{\Gamma_{21}}{\lambda\Gamma_{11}^2 + \Gamma_{21}^2} \\ \mu_5 = -\dfrac{\lambda\Gamma_{11}\Gamma_{12} + \Gamma_{21}\Gamma_{22}}{\lambda\Gamma_{11}^2 + \Gamma_{21}^2}. \end{cases} \tag{16}$$

Corresponding capacitor voltage and inductor current references in (15) can be calculated by using third-order Lagrange extrapolation strategy

$$\begin{cases} \bar{v}_f^*(k+1) = 4\bar{v}_f^*(k) - 6\bar{v}_f^*(k-1) + 4\bar{v}_f^*(k-2) - \bar{v}_f^*(k-3) \\ \bar{i}_f^*(k+1) = jC_f\omega_{\text{ref}}\bar{v}_f^*(k+1) + \bar{i}_g(k+1) \end{cases} \tag{17}$$

where $\bar{i}_g(k+1)$ can be replaced by $\bar{i}_g(k)$ for simplicity, since the load current can be considered as constant in a sampling period T_s.

Further, the second-order partial derivative of the CF is derived as

$$\frac{\partial^2 g_{dual}(v_{i\alpha}(k), v_{i\beta}(k))}{\partial v_{i\alpha}(k)^2} = \frac{\partial^2 g_{dual}(v_{i\alpha}(k), v_{i\beta}(k))}{\partial v_{i\beta}(k)^2} \qquad (18)$$
$$= 2(\lambda \Gamma_{11}^2 + \Gamma_{21}^2) > 0.$$

Since (18) is non-negative, (15) yields the unconstrained OVV that can minimize the CF. By introducing the inductor current tracking term into the CCS-based M^{2}PC, the voltage quality can be significantly improved in comparison to typical single-objective CCS-MPC. Another attractive feature of the proposed horizon-one M^{2}PC is that it inherits an advantage of the unconstrained CCS-MPC, i.e., offline precalculation, which reduces the online computational cost.

C. Control Delay and Dead-Time Compensation

Note that the calculated OVV in (15) is employed at the next sampling instant practically, resulting in one-step control delay [17]. This delay causes the deterioration of the system performance or even failure of M^{2}PC. To compensate this delay, a two-step prediction strategy is used [30], i.e., replacing the $(k+1)$th instant references and predictive values in (12) with their values at the time interval $k+2$. Correspondingly, the unconstrained OVV in (15) is rewritten as

$$\bar{v}_i^{\text{ref}}(k+1) = \mu_1 \bar{i}_f(k+1) + \mu_2 \bar{v}_f(k+1) + \mu_3 \bar{i}_f^*(k+2)$$
$$+ \mu_4 \bar{v}_f^*(k+2) + \mu_5 \bar{i}_g(k+1) \qquad (19)$$

where the references $\bar{i}_f^*(k+2)$ and $\bar{v}_f^*(k+2)$ are obtained from the one-step forward recursion of (17). The state predictions $\bar{i}_f(k+1)$ and $\bar{v}_f(k+1)$ are estimated by the predictive model (4) with the control input OVV calculated at the previous sampling period. $\bar{i}_g(k+1)$ can be replaced by $\bar{i}_g(k)$.

Additionally, in practical implementation, the dead time is usually necessary for short-circuit prevention. However, the dead-time effect causes undesired voltage deviation, degrading the tracking precision of M^{2}PC. To overcome this negative effect, a dead-time compensation strategy is utilized [31]. By online correcting the SVM pulses according to the three-phase inductor current polarity, the dead-time effect can be effectively compensated without adding extra hardware.

D. Constraints Reconsideration

FCS-MPC can handle the constraints by simply adding additional terms in CF [27]. However, for typical CCS-MPC, to include all the constraints, it often needs to solve a cumbersome QP problem, which requires heavy computational efforts to implement online. The explicit and implicit MPC can mitigate this problem, but they still have some generality and extension issues [25]. To this end, this paper introduces a simple 'online post-correction' solution to handle M^{2}PC with both inductor current and converter voltage vector constraints. The proposed solution can avoid solving the complex online QP problems or offline explicit solutions caused by various
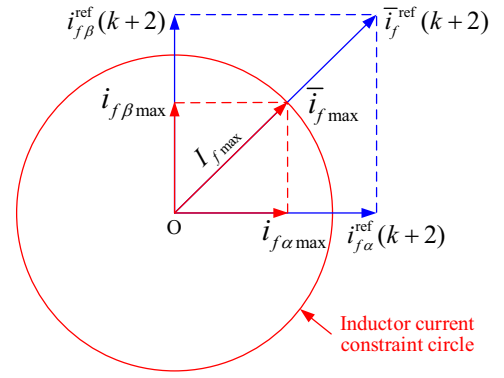

Fig. 3. Proposed solution to M^{2}PC with inductor current constraint.

constraints. It maximizes the merits of offline optimization of unconstrained situation and provides a more direct way to handle various constraints with a reduced computational cost compared with typical CCS-MPC. Its main idea is that based on the unconstrained OVV of M^{2}PC precalculated offline, reconsidering the constraints to correct the unconstrained OVV online, which is further elaborated as below.

1) Filter Inductor Current Constraint: Practically, limiting the inductor current to an allowed range is important for assuring hardware safety and avoiding the inductor core saturation. Specific design procedures of the proposed constraint-handling solution are given as follows.

Step 1: State Prediction. Considering the control delay compensation, applying the precalculated unconstrained OVV $\bar{v}_i^{ref}(k+1)$ in (19) to the two-step prediction model of (4), then the predicted inductor current is calculated as

$$\bar{i}_f^{\text{ref}}(k+2) = \Phi_{11} \bar{i}_f(k+1) + \Phi_{12} \bar{v}_f(k+1)$$
$$+ \Gamma_{11} \bar{v}_i^{\text{ref}}(k+1) + \Gamma_{12} \bar{i}_g(k+1). \qquad (20)$$

Step 2: State Constraint. Assuming that the allowed range of the inductor current magnitude is set as

$$\left| \bar{i}_f^{\text{ref}}(k+2) \right| = \sqrt{i_{f\alpha}^{\text{ref}}(k+2)^2 + i_{f\beta}^{\text{ref}}(k+2)^2} \leq I_{f\max} \quad (21)$$

where $I_{f\max}$ is the predefined maximum average value of the inductor current.

Step 3: Online Post-Correction. The core idea is to directly handle the inductor current constraint as shown in Fig. 3. To be specific, if the predicted $\left| \bar{i}_f^{\text{ref}}(k+2) \right| \leq I_{f\max}$, then $\bar{v}_i^{\text{ref}}(k+1)$ is kept unchanged. Otherwise, if $\left| \bar{i}_f^{\text{ref}}(k+2) \right| > I_{f\max}$, then $\bar{i}_f^{\text{ref}}(k+2)$ should be limited to its maximum value as

$$\bar{i}_{f\max} = \frac{\bar{i}_f^{\text{ref}}(k+2)}{\left| \bar{i}_f^{\text{ref}}(k+2) \right|} I_{f\max}. \qquad (22)$$

Correspondingly, the unconstrained OVV should be corrected as

$$\bar{v}_{i\lim} = \begin{cases} \bar{v}_i^{\text{ref}}(k+1), & \left| \bar{i}_f^{\text{ref}}(k+2) \right| \leq I_{f\max} \\ \dfrac{\bar{i}_{f\max} - \gamma}{\Gamma_{11}}, & \left| \bar{i}_f^{\text{ref}}(k+2) \right| > I_{f\max} \end{cases} \qquad (23)$$

where $\gamma = \Phi_{11} \bar{i}_f(k+1) + \Phi_{12} \bar{v}_f(k+1) + \Gamma_{12} \bar{i}_g(k+1)$.

TABLE I
COMPUTATIONS OF THE PROPOSED CONSTRAINED M²PC

Step No.	Equation No.	Multiplications (α, β)	Additions (α, β)
1	(15)	5×2	4×2
2	(20)	4×2	3×2
3	(21)	3	1
4	(22)	2×2	0
5	(23)	1×2	1×2
6	(24)	3	1
7	(25)	2×2	0
	Total:	34	18

Fig. 4. Implementation of proposed constrained M²PC scheme for an *LC*-filtered VSC.

TABLE II
NOMINAL PARAMETERS OF THE SYSTEM

Sampling period	$T_s = 50 \ \mu s$
DC bus voltage	$V_{DC} = 700$ V
Nominal *LC* filter	$L_f = 2.4$ mH, $C_f = 15 \ \mu F$
Switching frequency	$f_{sw} = 10$ kHz
VSC dead time	$T_d = 4 \ \mu s$
Linear load (resistance)	$R_l = 60 \ \Omega$
Nonlinear load	$R_n = 460 \ \Omega, C_n = 2.2$ mF, $L_n = 1.8$ mH
Reference voltage amplitude	$V_{\text{ref}} = 300$ V
Reference angular frequency	$\omega_{\text{ref}} = 100\pi$ rad/s

It is worth mentioning that the delay compensation is included in the proposed constraint-handling solution (23), since the calculation of $\bar{v}_i^{\text{ref}}(k+1)$ in (19) has already considered that. Then, future values of the inductor current can be limited within the predefined maximum value.

2) Converter voltage vector constraint: To avoid the over-modulation of SVM, the limit of the converter voltage vector (i.e., OVV) is considered as well. The converter voltage vector constraint is defined as follows

$$|\bar{v}_{i\,\text{lim}}| = \sqrt{v_{i\,\text{lim}\,\alpha}^2 + v_{i\,\text{lim}\,\beta}^2} \leq V_{\max} = \frac{V_{DC}}{\sqrt{3}} \quad (24)$$

where $V_{\max}$ is the allowed maximum amplitude of the OVV and V_{DC} is the dc bus voltage.

Similar to the principle in Fig. 3, the final form of the constrained OVV is described as

$$\bar{v}_{iop} = \begin{cases} \bar{v}_{i\,\text{lim}}, & |\bar{v}_{i\,\text{lim}}| \leq V_{\max} \\ \dfrac{\bar{v}_{i\,\text{lim}}}{|\bar{v}_{i\,\text{lim}}|} V_{\max}, & |\bar{v}_{i\,\text{lim}}| > V_{\max}. \end{cases} \quad (25)$$

Based on (23) and (25), the proposed solution can handle both inductor current and converter OVV constraints with a reduced computational cost in comparison to typical CCS-MPC. Theoretically, the proposed solution is applicable for any predictive model-based CCS-MPC scheme. Finally, the corrected constrained OVV $\bar{v}_{iop}$ is fed into the SVM module, resulting in a constant switching frequency.

E. Computational Cost

To demonstrate the proposed constrained M²PC can reduce the computational cost in comparison to the state of art of the CCS-MPC, the computational efforts of the proposed method, the implicit and explicit MPC in [25] are compared. In [25], for all of the three phases, the implicit MPC requires 81 multiplications and 66 additions. The explicit MPC requires 360 multiplications and 360 additions. Similarly, the maximum computations of the proposed constrained M²PC for both α and β frames are calculated in Table I. It is notable that [25] neglects the delay compensation when calculating the computations, for a fair comparison, we neglect this as well.

It is obvious from Table I that the total computations of the proposed constrained M²PC are the least, which are about 3 times faster than implicit MPC and 14 times faster than explicit MPC. It is worth mentioning that if the delay compensation is
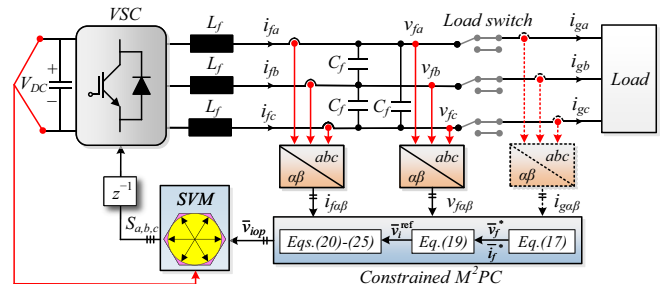
considered, the computations of the proposed method are still the least among the three methods.

Fig. 4 illustrates the implementation of the proposed constrained M²PC scheme for an *LC*-filtered VSC, where the capacitor voltage and the inductor current are directly measured. In this paper, the load current is measured for simplicity and it can be estimated by the state observer as well [2].

IV. WEIGHTING FACTOR SELECTION

1) Weighting Factor Selection: Parameters of the system are listed in Table II. Since the proposed M²PC is inherently a linear control strategy, the direct pole placement strategy is employed to determine the weighting factor λ in this paper.

To simplify the analysis, replacing $\bar{i}_f^*(k+1)$ in (15) with $\bar{v}_f^*(k+1)$ and $\bar{i}_g(k)$ in (17). Then, (15) is rearranged as

$$\bar{v}_i^{\text{ref}}(k) = \underbrace{\begin{bmatrix} \mu_1 & \mu_2 \end{bmatrix}}_{\mathbf{G}} \bar{\mathbf{x}}(k) + \underbrace{(\mu_4 + j\mu_3 C_f \omega_{\text{ref}})}_{H} \underbrace{\bar{v}_f^*(k+1)}_{u(k)}$$
$$+ \underbrace{(\mu_3 + \mu_5)}_{F} \bar{i}_g(k). \quad (26)$$

Note that the control delay is compensated by (19), hence, substituting (26) into the predictive model (4) yields the closed-loop dynamics of the proposed M²PC

$$\begin{cases} \bar{\mathbf{x}}(k+1) = \underbrace{(\mathbf{\Phi_d} + \mathbf{\Gamma_d G})}_{\mathbf{A_d}} \bar{\mathbf{x}}(k) + \underbrace{(\mathbf{\Gamma_d} H)}_{\mathbf{B_d}} u(k) + (\mathbf{\Gamma_{gd}} + \mathbf{\Gamma_d} F)\bar{i}_g(k) \\ \bar{y}(k) = \underbrace{\begin{bmatrix} 0 & 1 \end{bmatrix}}_{\mathbf{C_d}} \bar{\mathbf{x}}(k) = \bar{v}_f(k) \end{cases}$$
$$(27)$$

where $\mathbf{A_d}$, $\mathbf{B_d}$, $\mathbf{C_d}$ are the coefficient matrices. $\bar{y}(k)$ is the defined system output, i.e., the capacitor voltage.
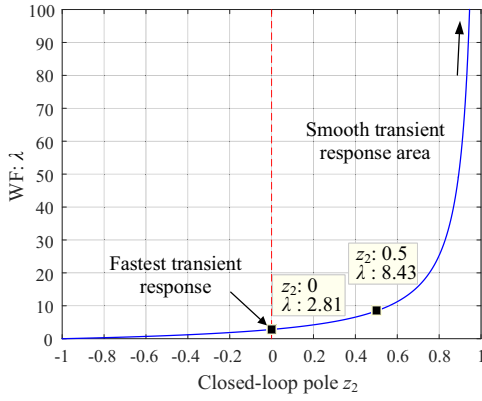
Fig. 5. Relationship between λ ($\lambda > 0$) and the pole z_2.

Further, (27) is converted into the discrete z-domain transfer function from the capacitor voltage reference to its feedback

$$G_{\mathrm{m}^2\mathrm{pc}}(z) = \mathbf{C_d}[z\mathbf{I} - \mathbf{A_d}]^{-1}\mathbf{B_d}$$
$$= \frac{(\Gamma_{21} + j\omega_{\mathrm{ref}}C_f\lambda\Gamma_{11})(\Gamma_{21}z - \Phi_{11}\Gamma_{21} + \Phi_{21}\Gamma_{11})}{\Delta} \quad (28)$$

where

$$\Delta = z((\lambda\Gamma_{11}{}^2 + \Gamma_{21}{}^2)z$$
$$+ \Gamma_{11}\Gamma_{21}(\lambda\Phi_{12} + \Phi_{21}) - \Phi_{11}\Gamma_{21}{}^2 - \lambda\Phi_{22}\Gamma_{11}{}^2). \quad (29)$$

It can be deduced from (28) and (29) that $G_{\mathrm{m}^2\mathrm{pc}}(z)$ contains one zero and two poles. Among them, one pole is $z_1 = 0$ and the other pole can be calculated as

$$z_2 = \frac{\lambda(\Phi_{22}\Gamma_{11}{}^2 - \Gamma_{11}\Gamma_{21}\Phi_{12}) - \Gamma_{11}\Gamma_{21}\Phi_{21} + \Phi_{11}\Gamma_{21}{}^2}{\lambda\Gamma_{11}{}^2 + \Gamma_{21}{}^2}. \quad (30)$$

Based on (30) and the nominal parameters in Table II, the relationship between λ ($\lambda > 0$) and the pole z_2 is shown in Fig. 5. It can be observed that λ increases with the increase of z_2, while the system is always stable since $z_2 = 1$ is the asymptote. To obtain a smooth transient performance, the WF is expected to be set as $\lambda \geq 2.81$. Meanwhile, a faster dynamic response and a higher stability margin can be obtained with a smaller λ (i.e., z_2 is closer to the origin). However, a tradeoff should be made between the dynamic response and the sensitivity to model mismatch in the actual implementation, e.g., z_2 can be placed at 0.5 with $\lambda = 8.43$ in this paper.

2) Sensitivity Analysis to Model Mismatch: With the parameters above, the closed loop zero-pole loci with actual inductance and capacitance uncertainties are depicted in Fig. 6 to evaluate the impact of the parameter mismatches on the proposed M^{2}PC. Fig. 6 (a) shows that the actual inductance varies from 62.1% to 200% of nominal L_f. It reflects that proposed controller is somewhat sensitive to the inductance mismatch, especially when the actual inductance is smaller than L_f, driving the dominant pole toward the unit circle. If the actual inductance decreases by more than $37.9\%L_f$, the closed-loop system becomes unstable. On the other hand, if the actual inductance is larger than L_f, the damping ratio is decreased and the overshoot is increased. Fig. 6 (b) shows that the actual capacitance varies from 50% to 200% of nominal C_f. It shows
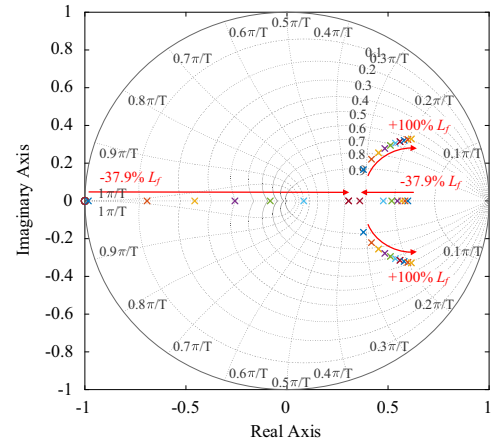

(a)
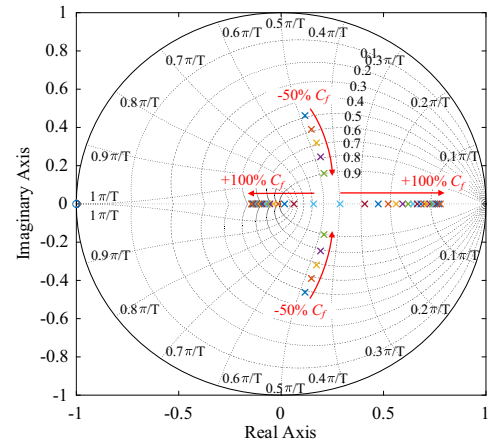
(b)

Fig. 6. Closed-loop zero-pole loci with model parameter mismatch. (a) Inductance uncertainties: $-37.9\%L_f$ to $+100\%L_f$. (b) Capacitance uncertainties: $-50\%C_f$ to $+100\%C_f$.

that a small actual capacitance reduces the damping ratio and drives the poles close to the unit circle, reducing the system stability. While a large actual capacitance deteriorates the dynamic response. To further enhance the robustness against the model mismatch of the proposed controller, λ can be further increased. Notably, this may also degrade the transient response. A simple prediction error correction strategy can be used to effectively mitigate this issue by feeding the prediction error term into (11) for compensation [32].

V. EXPERIMENTAL RESULTS

Experiments are carried out to verify the proposed constrained M^{2}PC. The experimental setup is depicted in Fig. 7(a), which comprises the dc power sources, an LC-filtered three-phase VSC and the linear/nonlinear load. The topology of the diode-rectifier nonlinear load is shown in Fig. 7(b). The proposed control algorism is implemented in dSPACE DS1202 board. In addition, comparative tests using the modified FCS-MPC in [27] and typical single-objective CCS-MPC (i.e., by directly setting λ in (11) and (16) to be 0) are carried out to justify the superiority of the presented control scheme. For a fair comparison, the sampling period of the modified
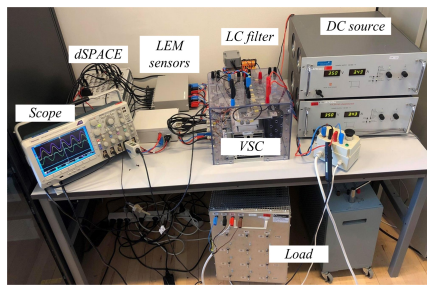
(a)
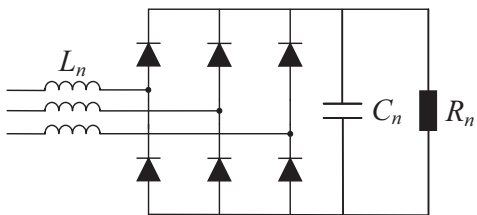
(b)

Fig. 7. Experimental setup to validate the proposed control scheme. (a) Experimental setup. (b) Diode-rectifier nonlinear load.

TABLE III
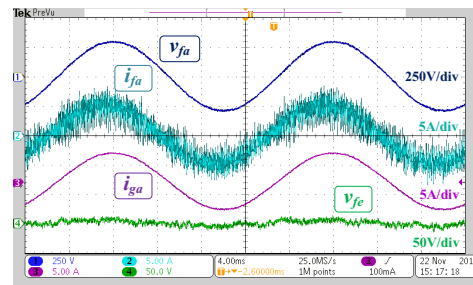COMPARISON OF VOLTAGE TRACKING RMSE OF THREE METHODS

Control Type	RMSE (Linear load)	RMSE (Nonlinear load)
Modified FCS-MPC	4.372 V	3.819 V
Typical CCS-MPC	4.593 V	4.203 V
Proposed constrained M^2PC	2.543 V	1.765 V

(a)

(b)

(c)

Fig. 8. Experimental comparisons: steady-state responses of v_{fa}, i_{fa}, i_{ga} and voltage tracking error v_{fe} with linear load. (V_{ref} = 300 V, R_l = 60 Ω). (a) Modified FCS-MPC. (THD of v_{fa}: 1.57%). (b) Typical CCS-MPC. (THD of v_{fa}: 2.23%). (c) Proposed M^2PC. (THD of v_{fa}: 1.16%).

FCS-MPC is chosen as 20 μs, which can obtain an average switching frequency of about 10 kHz [29], [33]. The sampling period of the typical CCS-MPC is 50 μs, which is the same with that of the proposed M^2PC.
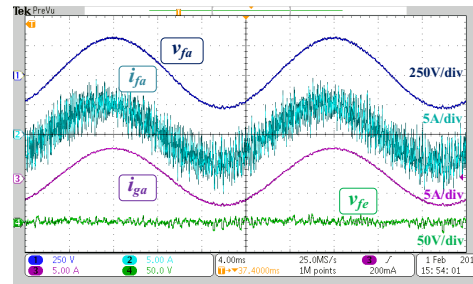
In addition, to compare the computational burden between the proposed M^2PC and the modified FCS-MPC, the turnaround time in one sampling interval is calculated. The turnaround time of the modified FCS-MPC is 15 μs, including 12 μs AD conversion time and 3 μs algorithm execution time [33]. Similarly, the turnaround time of the proposed method is 16 μs, which is comparable with that of the modified FCS-MPC. This means the proposed method is very computationally efficient. Moreover, both methods can be completed in one sampling period.

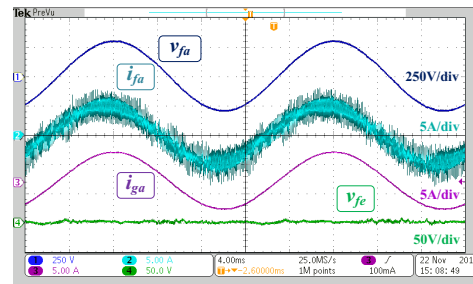### A. Performance Evaluation of Proposed M^2PC

Fig. 8 depicts the experimental results of the steady-state performance feeding nominal linear load (60 Ω) with the modified FCS-MPC in [27], typical CCS-MPC and the proposed M^2PC, where the phase voltage feedback v_{fa}, inductor current i_{fa}, load current i_{ga} and phase voltage tracking error v_{fe} are given. It shows that the proposed M^2PC offers the best voltage tracking response with the lowest THD and steady-state error among the three methods. The modified FCS-MPC has a little worse performance than the proposed M^2PC due to the lack of the modulator. In contrast, even with a modulator,

the typical CCS-MPC still behaves the worst. This is because it neglects the coupling effects of the *LC* filter, resulting in a large voltage oscillation. These results reveal that the proposed M^2PC exhibits a better steady-state voltage tracking performance than both modified FCS-MPC and typical CCS-MPC under the linear load condition.

Fig. 9 shows the experimental results of the steady-state performance under nonlinear load with modified FCS-MPC, typical CCS-MPC and proposed M^2PC, where the reference phase voltage v_{fa}^*, feedback phase voltage v_{fa}, load current i_{ga} and phase voltage tracking error v_{fe} are given. It can be seen that there are no obvious phase voltage distortions of the three methods. Similarly, the THD and the steady-state error with the proposed M^2PC are still the lowest among the three methods. Hence, under the same nonlinear load condition, superior voltage quality can be obtained by using the proposed M^2PC scheme. Additionally, it is worth mentioning that the THD of the modified FCS-MPC decreases from 1.57 % with linear load to 1.52 % with non-linear load. This is because the average switching frequency of the modified FCS-MPC raises from 9.6 kHz to 10.2 kHz when supplying the nonlinear load,
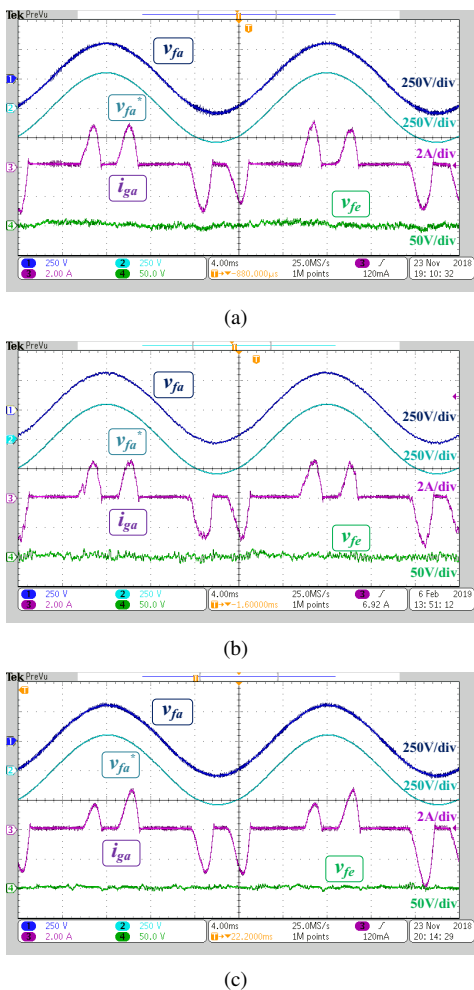
Fig. 9. Experimental comparisons: steady-state responses of v_{fa}, i_{ga} and voltage tracking error v_{fe} with nonlinear load. (V_{ref} = 300 V). (a) Modified FCS-MPC. (THD of v_{fa}: 1.52%). (b) Typical CCS-MPC. (THD of v_{fa}: 2.12%). (c) Proposed M^{2}PC. (THD of v_{fa}: 1.20%).
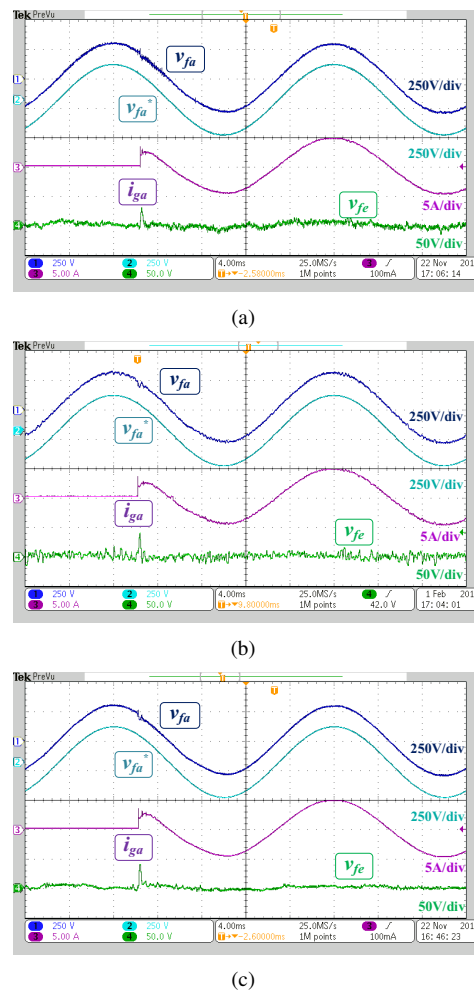

Fig. 10. Experimental comparisons: transient responses of v_{fa}, i_{ga} and v_{fe} with linear load step change. (V_{ref} = 300 V, R_l: open circuit to 60 Ω). (a) Modified FCS-MPC. (b) Typical CCS-MPC. (c) Proposed M^{2}PC.

resulting the decrease of the THD.

To quantitatively compare the steady-state tracking performance of the modified FCS-MPC, typical CCS-MPC and the proposed M^{2}PC, the root mean square error (RMSE) of the phase voltage is used, which is calculated as follows

$$\text{RMSE}(v_{fa}^* - v_{fa}) = \sqrt{\frac{1}{N}\sum_{i=1}^{N}(v_{fa,i}^* - v_{fa,i})^2} \quad (31)$$

where N is the total number of the sampling points. $v_{fa,i}^*$ and $v_{fa,i}$ are phase voltage reference and feedback, respectively.

Corresponding experimental comparisons of the voltage tracking RMSE of the three methods are listed in Table III. Same conclusions can be drawn that the proposed M^{2}PC has the smallest voltage tracking RMSE among the three methods both under linear and nonlinear load condition, resulting the best steady-state voltage tracking performance.

Fig. 10 shows the experimental comparisons of the transient performance with linear load step change (from open circuit to 60 Ω) using modified FCS-MPC, typical CCS-MPC and proposed M^{2}PC, where the reference and feedback phase

voltage v_{fa}^* and v_{fa}, the load current i_{ga} and the phase voltage tracking error v_{fe} are given. Fig. 11 depicts the corresponding IEC 62040 standard. It is exhibited in Fig. 10 that the modified FCS-MPC offers a slightly better robustness than typical CCS-MPC and proposed M^{2}PC with a lower voltage fluctuation in the transient process. However, its sampling frequency is also much higher, resulting in a higher bandwidth and increased hardware cost. The robustness against the load step change of typical CCS-MPC and proposed M^{2}PC is similar. Additionally, it is clearly shown in Fig. 11 that the transient voltage tracking errors of three methods conform significantly well with the IEC 62040 standard.

In addition, to investigate the sensitivity to parameter mismatch of the proposed M^{2}PC, quantitative experimental comparisons of the phase voltage RMSE and THD under actual inductance and capacitance mismatches are illustrated in Table IV with a linear load. It shows that the steady-state performance of the proposed method is affected by the model mismatch to a varying degree. As expected, when the actual inductance is smaller than the nominal value, the RMSE and THD are somewhat increased. On the other hand, a large actual capacitance does not have a significant impact on the THD,
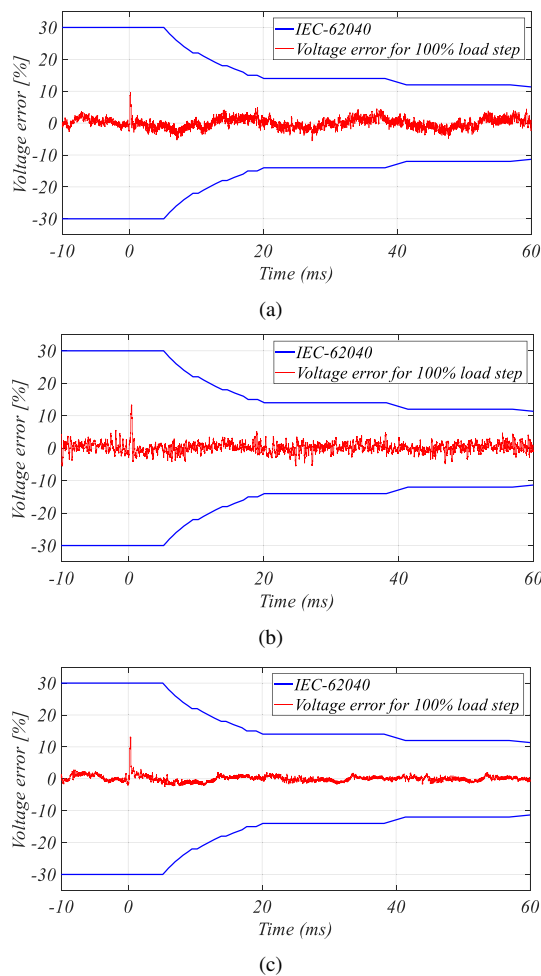
Fig. 11. Experimental comparisons: transient response of voltage tracking errors for 100% step change of linear load according to IEC 62040 standard. (a) Modified FCS-MPC. (b) Typical CCS-MPC. (c) Proposed M^2PC.

Fig. 12. Experimental results for validation of the proposed solution to handle constraints. (V_{ref} = 0-300 V, R_l = 60 Ω). (a) Without proposed solution. (b) With proposed solution without delay compensation. (c) With proposed solution with delay compensation.

TABLE IV
SENSITIVITY TO MODEL MISMATCH OF PROPOSED M^2PC

Parameter Uncertainties	Voltage RMSE (V)	THD (%)
$-35\%L_f$ and C_f	6.986	2.25
L_f and $-50\%C_f$	4.799	1.36
$+100\%L_f$ and C_f	3.419	1.81
L_f and $+100\%C_f$	7.430	0.99
$-35\%L_f$ and $-50\%C_f$	10.173	3.31
$-35\%L_f$ and $+100\%C_f$	7.598	1.95
$+100\%L_f$ and $-50\%C_f$	4.315	2.10
$+100\%L_f$ and $+100\%C_f$	8.793	1.20

whereas the voltage RMSE is somewhat increased due to the slow dynamic response. The worst case is that both actual inductance and capacitance are overestimated by the nominal ones, resulting in a worst performance. It is worth mentioning that the steady-state performance of the proposed method under the most cases of the model mismatch are acceptable with the RMSE less than 3% and THD less than 2%.
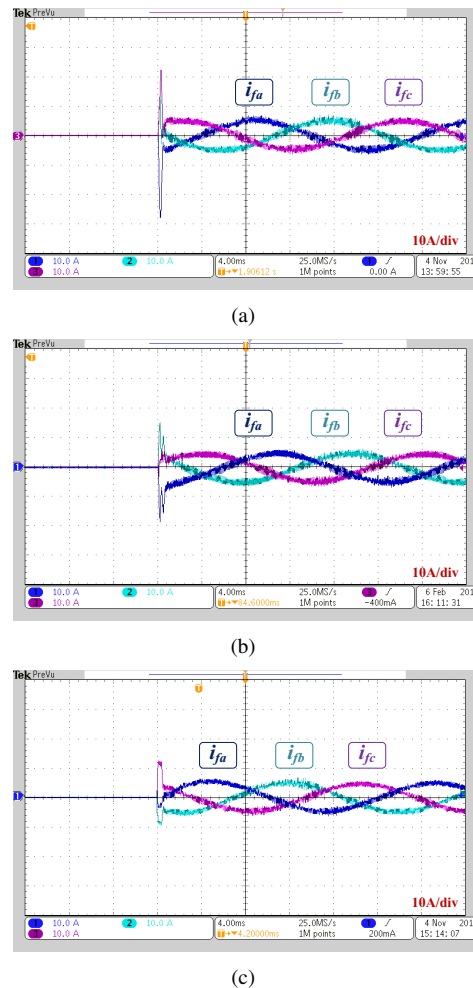
B. Verification of Proposed Constraint-Handling Solution

The experimental results for validating the proposed constraint-handling solution are illustrated in Fig. 12, where the starting responses of the three-phase inductor current without the proposed solution, with the proposed solution without delay compensation and with the proposed solution with delay compensation are given, respectively. The inductor current constraint $I_{f\max}$ is set as 12 A considering the inductor core saturation and hardware safety. It can be seen that without using the proposed constraint-handling solution, the inductor current tends to sharply increase to a high value during the starting process. When using the proposed solution while neglecting the delay compensation, the inductor current still cannot be accurately limited to the predefined value, which indicates that the delay compensation is necessary in the actual implementation of the proposed solution. In contrast, by employing the proposed 'online post-correction' solution with delay compensation, the inductor current is successfully limited to the predefined value. In addition, it is worth mentioning that the inductor current ripple may slightly exceed the predefined constraint due to the use of the state space

averaging based predictive model.

VI. Conclusion

A constrained M^2PC scheme for LC-filtered VSCs has been presented in this paper. First, a dual-objective CF is introduced to the proposed CCS-based M^2PC, where the inductor current tracking objective is included as an 'equally important term', resulting in an improved voltage quality. The proposed M^2PC generates the unconstrained OVV by calculating the minimum analytical solution of the CF offline. Moreover, a simple 'online post-correction' strategy is reconsidered to handle the various constraints and the generated OVV is synthesized by SVM, achieving the fixed switching frequency and low THD. Compared with typical CCS-MPC, the proposed control scheme can significantly reduce the computational burden. In addition, the WF selection procedures and the sensitivity to the model mismatch are analyzed. Experimental results have verified the proposed control strategy.

References

[1] J. Rocabert, A. Luna, F. Blaabjerg, and P. Rodríguez, "Control of power converters in AC microgrids," *IEEE Trans. Power Electron.*, vol. 27, no. 11, pp. 4734–4749, Nov. 2012.

[2] P. Cortés, G. Ortiz, J. I. Yuz, J. Rodríguez, S. Vazquez, and L. G. Franquelo, "Model predictive control of an inverter with output LC filter for UPS applications," *IEEE Trans. Ind. Electron.*, vol. 56, no. 6, pp. 1875–1883, Jun. 2009.

[3] T. Dragičević, X. Lu, J. C. Vasquez, and J. M. Guerrero, "DC microgrids - part II: a review of power architectures, applications, and standardization issues," *IEEE Trans. Power Electron.*, vol. 31, no. 5, pp. 3528–3549, May. 2016.

[4] Poh Chiang Loh, M. Newman, D. Zmood, and D. Holmes, "A comparative analysis of multiloop voltage regulation strategies for single and three-phase UPS systems," *IEEE Trans. Power Electron.*, vol. 18, no. 5, pp. 1176–1185, Sep. 2003.

[5] D. N. Zmood and D. G. Holmes, "Stationary frame current regulation of PWM inverters with zero steady-state error," *IEEE Trans. Power Electron.*, vol. 18, no. 3, pp. 814–822, May. 2003.

[6] O. Kukrer, "Deadbeat control of a three-phase inverter with an output LC filter," *IEEE Trans. Power Electron.*, vol. 11, no. 1, pp. 16–23, 1996.

[7] L. Zheng, F. Jiang, J. Song, Y. Gao, and M. Tian, "A discrete-time repetitive sliding mode control for voltage source inverters," *IEEE J. Emerg. Sel. Top. Power Electron.*, vol. 6, no. 3, pp. 1553–1566, Sep. 2018.

[8] S. Kouro, P. Cortes, R. Vargas, U. Ammann, and J. Rodriguez, "Model predictive control—a simple and powerful method to control power converters," *IEEE Trans. Ind. Electron.*, vol. 56, no. 6, pp. 1826–1838, Jun. 2009.

[9] C. Bordons and C. Montero, "Basic principles of MPC for power converters: bridging the gap between theory and practice," *IEEE Ind. Electron. Mag.*, vol. 9, no. 3, pp. 31–43, Sep. 2015.

[10] C. Zheng, T. Dragicevic, and F. Blaabjerg, "Current-sensorless finite-set model predictive control for LC-filtered voltage source inverters," *IEEE Trans. Power Electron.*, to be published, doi: 10.1109/TPEL.2019.2914452.

[11] S. Vazquez, J. Rodriguez, M. Rivera, L. G. Franquelo, and M. Norambuena, "Model predictive control for power converters and drives: advances and trends," *IEEE Trans. Ind. Electron.*, vol. 64, no. 2, pp. 935–947, Feb. 2017.

[12] Z. Song, Y. Tian, W. Chen, Z. Zou, and Z. Chen, "Predictive duty cycle control of three-phase active-front-end rectifiers," *IEEE Trans. Power Electron.*, vol. 31, no. 1, pp. 698–710, Jan. 2016.

[13] T. Dragicevic, C. Zheng, J. Rodriguez, and F. Blaabjerg, "Robust quasi-predictive control of LCL-filtered grid converters," *IEEE Trans. Power Electron.*, to be published, doi: 10.1109/TPEL.2019.2916604.

[14] M. Siami, D. Arab Khaburi, and J. Rodriguez, "Simplified finite control set-model predictive control for matrix converter-fed PMSM drives," *IEEE Trans. Power Electron.*, vol. 33, no. 3, pp. 2438–2446, Mar. 2018.

[15] T. Dragicevic, "Dynamic stabilization of DC microgrids with predictive control of point-of-load converters," *IEEE Trans. Power Electron.*, vol. 33, no. 12, pp. 10 872–10 884, Dec. 2018.

[16] S. Vazquez, R. P. Aguilera, P. Acuna, J. Pou, J. I. Leon, L. G. Franquelo, and V. G. Agelidis, "Model predictive control for single-phase NPC converters based on optimal switching sequences," *IEEE Trans. Ind. Electron.*, vol. 63, no. 12, pp. 7533–7541, Dec. 2016.

[17] P. Cortes, J. Rodriguez, D. E. Quevedo, and C. Silva, "Predictive current control strategy with imposed load current spectrum," *IEEE Trans. Power Electron.*, vol. 23, no. 2, pp. 612–618, Mar. 2008.

[18] L. Tarisciotti, P. Zanchetta, A. Watson, S. Bifaretti, and J. C. Clare, "Modulated model predictive control for a seven-level cascaded H-bridge back-to-back converter," *IEEE Trans. Ind. Electron.*, vol. 61, no. 10, pp. 5375–5383, Oct. 2014.

[19] M. Tomlinson, H. d. T. Mouton, R. Kennel, and P. Stolze, "A fixed switching frequency scheme for finite-control-set model predictive control—concept and algorithm," *IEEE Trans. Ind. Electron.*, vol. 63, no. 12, pp. 7662–7670, Dec. 2016.

[20] R. P. Aguilera, P. Lezana, and D. E. Quevedo, "Finite-control-set model predictive control with improved steady-state performance," *IEEE Trans. Ind. Informatics*, vol. 9, no. 2, pp. 658–667, May. 2013.

[21] F. Sebaaly, H. Vahedi, H. Y. Kanaan, and K. Al-Haddad, "Novel current controller based on MPC with fixed switching frequency operation for a grid-tied inverter," *IEEE Trans. Ind. Electron.*, vol. 65, no. 8, pp. 6198–6205, Aug. 2018.

[22] M. G. Judewicz, S. A. Gonzalez, N. I. Echeverria, J. R. Fischer, and D. O. Carrica, "Generalized predictive current control (GPCC) for grid-tie three-phase inverters," *IEEE Trans. Ind. Electron.*, vol. 63, no. 7, pp. 4475–4484, Jul. 2016.

[23] S. Mariethoz and M. Morari, "Explicit model-predictive control of a PWM inverter with an LCL filter," *IEEE Trans. Ind. Electron.*, vol. 56, no. 2, pp. 389–399, Feb. 2009.

[24] M. N. Zeilinger, C. N. Jones, and M. Morari, "Real-time suboptimal model predictive control using a combination of explicit MPC and online optimization," *IEEE Trans. Automat. Contr.*, vol. 56, no. 7, pp. 1524–1534, Jul. 2011.

[25] M. Nauman and A. Hasan, "Efficient implicit model-predictive control of a three-phase inverter with an output LC filter," *IEEE Trans. Power Electron.*, vol. 31, no. 9, pp. 6075–6078, Sep. 2016.

[26] P. Cortes, S. Kouro, B. La Rocca, R. Vargas, J. Rodriguez, J. I. Leon, S. Vazquez, and L. G. Franquelo, "Guidelines for weighting factors design in model predictive control of power converters and drives," in *2009 IEEE Int. Conf. Ind. Technol.* IEEE, Feb. 2009, pp. 1–7.

[27] T. Dragicevic, "Model predictive control of power converters for robust and fast operation of ac microgrids," *IEEE Trans. Power Electron.*, vol. 33, no. 7, pp. 6304–6317, Jul. 2018.

[28] F. Villarroel, J. R. Espinoza, C. A. Rojas, J. Rodriguez, M. Rivera, and D. Sbarbaro, "Multiobjective switching state selector for finite-states model predictive control based on fuzzy decision making in a matrix converter," *IEEE Trans. Ind. Electron.*, vol. 60, no. 2, pp. 589–599, Feb. 2013.

[29] T. Dragicevic and M. Novak, "Weighting factor design in model predictive control of power electronic converters: an artificial neural network approach," *IEEE Trans. Ind. Electron.*, to be published, doi: 10.1109/TIE.2018.2875660.

[30] P. Cortes, J. Rodriguez, C. Silva, and A. Flores, "Delay compensation in model predictive current control of a three-phase inverter," *IEEE Trans. Ind. Electron.*, vol. 59, no. 2, pp. 1323–1325, Feb. 2012.

[31] Jong-Lick Lin, "A new approach of dead-time compensation for PWM voltage inverters," *IEEE Trans. Circuits Syst. I Fundam. Theory Appl.*, vol. 49, no. 4, pp. 476–483, Apr. 2002.

[32] M. Siami, D. A. Khaburi, A. Abbaszadeh, and J. Rodriguez, "Robustness improvement of predictive current control using prediction error correction for permanent-magnet synchronous machines," *IEEE Trans. Ind. Electron.*, vol. 63, no. 6, pp. 3458–3466, Jun. 2016.

[33] M. Novak, U. M. Nyman, T. Dragicevic, and F. Blaabjerg, "Analytical design and performance validation of finite set MPC regulated power converters," *IEEE Trans. Ind. Electron.*, vol. 66, no. 3, pp. 2004–2014, Mar. 2019.

Changming Zheng (S'19) received the B.Sc. degree in the College of Information and Control Engineering, China University of Petroleum (East China), Qingdao, China, in 2014, where he is currently working toward the Ph.D. degree in power electronics. He is also a Visiting Ph.D. Student with the Department of Energy Technology, Aalborg University, Aalborg, Denmark, since 2018.

His research interests include model predictive control, power converters control in renewable energy systems, AC microgrids and permanent magnet synchronous motor drives.

Tomislav Dragičević (S'09-M'13-SM'17) received the M.Sc. and the industrial Ph.D. degrees in Electrical Engineering from the Faculty of Electrical Engineering, Zagreb, Croatia, in 2009 and 2013, respectively. From 2013 until 2016 he has been a Postdoctoral research associate at Aalborg University, Denmark. From March 2016 he is an Associate Professor at Aalborg University, Denmark where he leads an Advanced Control Lab. He made a guest professor stay at Nottingham University, UK during spring/summer of 2018. His principal field of interest is design and control of microgrids, and application of advanced modeling and control concepts to power electronic systems. He has authored and co-authored more than 155 technical papers (more than 70 of them are published in international journals, mostly IEEE Transactions) in his domain of interest, 8 book chapters and a book in the field. He serves as Associate Editor in the IEEE TRANSACTIONS ON INDUSTRIAL ELECTRONICS, in IEEE Emerging and Selected Topics in Power Electronics and in IEEE Industrial Electronics Magazine. Dr. Dragičević is a recipient of the Končar prize for the best industrial PhD thesis in Croatia, and a Robert Mayer Energy Conservation award.

Branko Majmunović (S'18) received the B.S. degree in electrical engineering from the University of Belgrade, Belgrade, Serbia in 2016, and the M.S. degree in power electronics and drives from Aalborg University, Aalborg, Denmark, in 2018. He is currently working toward the Ph.D. degree at the Department of Electrical, Computer and Energy Engineering, University of Colorado, Boulder. His research interests include modular grid-tied power electronics.

Frede Blaabjerg (S'86–M'88–SM'97–F'03) was with ABB-Scandia, Randers, Denmark, from 1987 to 1988. From 1988 to 1992, he got the PhD degree in Electrical Engineering at Aalborg University in 1995. He became an Assistant Professor in 1992, an Associate Professor in 1996, and a Full Professor of power electronics and drives in 1998. From 2017 he became a Villum Investigator. He is honoris causa at University Politehnica Timisoara (UPT), Romania and Tallinn Technical University (TTU) in Estonia.

His current research interests include power electronics and its applications such as in wind turbines, PV systems, reliability, harmonics and adjustable speed drives. He has published more than 600 journal papers in the fields of power electronics and its applications. He is the co-author of four monographs and editor of ten books in power electronics and its applications.

He has received 30 IEEE Prize Paper Awards, the IEEE PELS Distinguished Service Award in 2009, the EPE-PEMC Council Award in 2010, the IEEE William E. Newell Power Electronics Award 2014 and the Villum Kann Rasmussen Research Award 2014. He was the Editor-in-Chief of the IEEE TRANSACTIONS ON POWER ELECTRONICS from 2006 to 2012. He has been Distinguished Lecturer for the IEEE Power Electronics Society from 2005 to 2007 and for the IEEE Industry Applications Society from 2010 to 2011 as well as 2017 to 2018. In 2019-2020 he serves a President of IEEE Power Electronics Society. He is Vice-President of the Danish Academy of Technical Sciences too. He is nominated in 2014-2018 by Thomson Reuters to be between the most 250 cited researchers in Engineering in the world.